

## NUMERICAL STUDY OF EFFICIENCY OF MULTI-TURN EXTRACTION IN THE K1200 CYCLOTRON

H. BLOSSER, D. JOHNSON, F. MARTI

*National Superconducting Cyclotron Laboratory  
Michigan State University, East Lansing, MI 48824-1321 USA*

The K1200 cyclotron at NSCL normally operates with a broad phase beam in order to achieve the highest possible intensity for production of secondary radioactive beams. Achieved extraction efficiencies of 30 to 70% are considerably lower than the 90% level assumed in performance estimates for the Coupled Cyclotron Project (CCP) – this paper reports results of an extensive set of numerical studies of factors determining the efficiency of such a multi-turn system. The results indicate coherent and incoherent axial and radial amplitudes to be dominant factors effecting the efficiency whereas the phase width of the rf group and the voltage stability of the rf system have surprisingly little effect. Septum thickness and septum shape are important factors but behave largely as expected on the basis of straightforward geometrical considerations.

### 1 Introduction

In compact superconducting cyclotrons, extraction of high intensity beams in the single-turn mode is generally not possible due to the energy spread induced in the single turn phase groups by the longitudinal space charge force[1]. Such cyclotrons therefore operate in the multi-turn mode when the highest intensities are needed, and extraction efficiency in many cases is the limiting factor determining the final intensity. (High extraction efficiency is obviously also desirable from the perspective of minimizing activation of the cyclotron and reducing radiation exposure to maintenance personnel.)

Extraction efficiencies routinely achieved in the multi-turn mode in the NSCL K1200 cyclotron range from 30 to 70%[2], whereas the PSI Injector I achieved a 93% efficiency in the multi-turn mode [3] and a previous very detailed numerical study of a 200  $\mu\text{A}$ , 250 MeV superconducting proton cyclotron indicated an efficiency of 95%[4]. The study reported here applies the computing techniques utilized for the previous proton cyclotron study to the K1200 in an effort to identify the specific factors leading to the low measured efficiencies.

### 2 Calculation Procedure

The initial goal of this study was to determine whether detailed numerical calculations of orbit behavior in the K1200 would produce extraction efficiencies matching the experimentally observed values. Thus far the studies have used a single main magnetic field corresponding to one of the most frequently used K1200 beams namely  $^{18}\text{O}^{6+}$  accelerated to 80 MeV/A. The magnetic field for the study is derived from the original field mapping data set for the K1200 and includes main field, trim coil fields, and imperfection fields, with main and trim coil currents set at the operating values used in actual cyclotron runs. This field data set is the most realistic description available of the actual field in the cyclotron.

#### 2.1 Central Ray Tracking

Orbit calculations begin with tracking of a family of 21 “central ray” trajectories covering the range of starting times (relative to the rf voltage) from  $200^\circ$  through  $220^\circ$  (where peak accelerating voltage is at  $270^\circ$ ). Initially the 21 central rays are tracked with the orbit code “Cyclone” which in the central region uses detailed electric field maps in addition to the usual magnetic maps. (After approximately 10 turns the energy gain computation shifts to an impulse approximation when electric field details are no longer significant.) Central rays start at the center of the exit aperture of the spiral inflector and are tracked through some 800 turns, stopping when the radius of a given ray (at the deflector entrance azimuth) exceeds that of the small r side of the deflector septum.

Figure 1 shows an  $(r, p_r)$  plot of the 21 central rays in the region near the extraction septum. (Throughout this paper,  $p_r$  represents the canonical radial momentum  $P_r$  multiplied by  $1/qB_0$ , where  $q$  is the ion charge and  $B_0$  is the magnetic field unit (usually the isochronous field at  $r = 0$ ); this multiplication makes  $p_r$  dimensionally a length which can then be put into any convenient length unit; if  $r$  and  $p_r$  are expressed in the same units, i.e. inches in the MSU orbit codes, the overall choice has the convenience of making eigen-ellipses approximately circular i.e. a displacement in  $p_r$  becomes a displacement in  $r$  of about the same amplitude after a radial oscillation phase advance of  $90^\circ$ .)

In setting up the magnetic field for calculations of “well-centered” beams, the K1200 centering coils have been adjusted to produce nearly perfect centering for the  $210^\circ$  ray at the center of the phase group, (evidenced by the complete absence of a coherent radial oscillation for this ray in the radius range from 38 to 39.2 inches). The other, time displaced, central rays in contrast show increasing precession due to phase dependent centering effects in the central region. As the radius reaches 39.4 inches the family of curves shows a standard precessional extraction pattern, namely, they develop a coherent radial oscillation amplitude due to the “extraction field bump” as

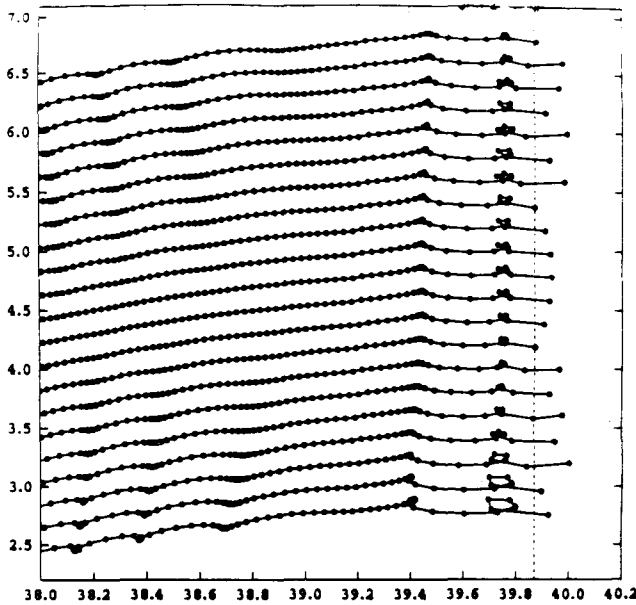


Figure 1: Plot at  $\theta = 30^\circ$  of  $p_r$  vs.  $r$  (both in inches -- see text for explanation of units) for 21 central ray orbits as they approach the extraction region. The orbits leave the center of the spiral inflector in the straight ahead direction at starting times in rf degrees of 200, 201, ..., 220. Note that the  $p_r$  scale is compressed relative to the  $r$  scale and the 201, 202, ..., 220 orbits are successively displaced by 0.2" increments relative to the 200° orbit. Starting point energy for all rays is 4.45 keV/A.

they pass through the  $v_r = 1$  resonance. In the Figure 1 calculation, the rf frequency and voltage have been adjusted so that the 210° ray and its six nearest neighbors all exceed the septum radius cut-off on the 808<sup>th</sup> turn, the next four further away rays (two on each side) require 809 turns, the next four 810, etc.

### 2.2 Transverse Phase Space Distribution

Effects of the incoherent radial and axial oscillations are included in the calculation beginning on the 708<sup>th</sup> turn (i.e. about 40 turns back from the beginning point of the plots in Figure 1). At this point displaced rays are added in sets of 8, equally spaced on eigen-ellipses of full area 3 & 12 mm-mr (i.e.  $0.95 \pi$  &  $3.82 \pi$  respectively) in either the radial or the axial plane or both. These groups of displaced rays are designated by the labels "small r", "large r" etc. The calculation at this point also shifts to the "Z4 Spiral Gap" code, which includes non-linear terms through 4<sup>th</sup> order in a symplectic formulation which includes all coupling terms[4]. The most frequently used ray tracking ensemble is the 1785 ray "small r, large r, small z" set i.e.  $(8+8+1) \times (4+1) \times (21)$  for radial, axial, and starting time distributions respectively. If extraction efficiency is computed giving equal weight to each of the 1785 rays, the 8+8+1 term corresponds to a presumed density peak or hot core in the radial phase space distribution, and similarly for the 4+1 term for the axial distribution, whereas the equal weighting of the 21 time points corresponds to an assumed square wave in this dimension. (The 4 in the axial term reflects the exact median plane symmetry assumed in

the calculation, so that opposite  $z$ ,  $p_z$  pairs are always related by a sign change and an 8 point eigen-ellipse reduces to 4 independent rays.)

Figure 2 shows the last 8 turns of the "210°, small r, median plane" sub-group of the overall ensemble – even this simplest group is seen to display significant non-linearities as successive turns move through the final coherent precession loop. The Figure also shows what would be needed to achieve single turn extraction in the K1200 – the last turn of the 3 mm-mr ellipse is separated from the previous turns by 1.2 mm. If spreading of the radial group from the combined effects of time spread, longitudinal space charge, coupling from the axial motion, and time jitter in magnet or rf is less than this value, single turn extraction would result. (This single-turn requirement appears to be incompatible with the high current beams expected in the coupled operation mode[6], but might be achieved at low currents with careful tuning.)

### 2.3 Broad Phase, Multi-turn Extraction Results

In the broad phase mode mainly used in the K1200 the turn structure is rather fully wiped out by the many overlapping turns as shown in Figure 3, which is a histogram of number of rays vs. radius. The dotted line at 39.87" marks the "small r" side of the deflector entry which we refer to hereafter as simply the "septum cutoff". Inside this cutoff, a given ray may appear more than once in a given  $r$  bin if its radial oscillation is large enough to give a negative radius gain over part of a precession cycle – beyond the septum cutoff, tracking stops when a ray first exceeds the cutoff radius (and the ray is transferred to the "Septum Penetration Code"). Thus all rays appear at most once in a radial bin in this radius interval. (In the runs with large  $r$  &  $z$  amplitudes, a few rays fail to reach the septum radius because they exceed aperture limits on some earlier turn, which also stops the tracking.)

In the Septum Penetration code the septum thickness can be set at any desired value. A thickness of 0.5 mm is thought to correspond to a typical K1200 operating situation (0.25mm being the physical thickness of the most

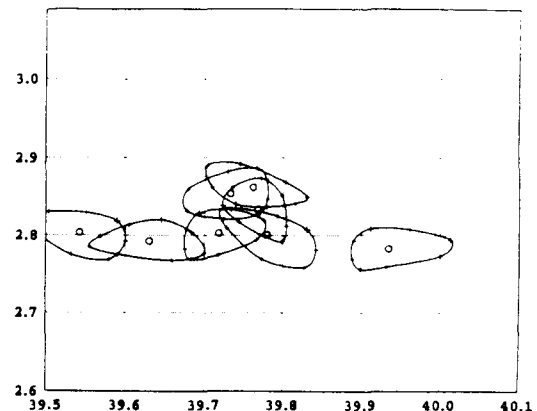


Figure 2: Plot of the 801<sup>st</sup> through 808<sup>th</sup> turns of the 210° orbit from Figure 1 with a 3 mm-mr eigenellipse added at  $E/A = 70.61$  MeV/A. the separation between turns 807 and 808 is approximately 1.4mm.

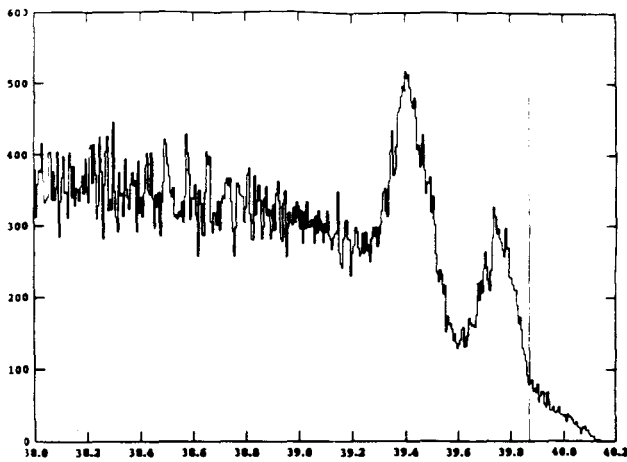


Figure 3: Histogram of number of rays crossing  $\theta = 30^\circ$  per 5.5 mil (0.14 mm) radial bin plotted vs radius (inches) for the K1200 80 MeV,  $Q/A = .33341$  field. The 1785 ray set includes "small r, large r, small z" distributions and the full  $20^\circ$  starting time distribution. See text for full definitions. Vertical line at 39.87" marks deflector septum location.

frequently used septa and an additional 0.25 mm is added to represent fabrication and alignment errors). With this thickness 395 rays (22.1%) of the 1785 ray group from Figure 3 hit the septum of the first electrostatic deflector (E1) (most of these at the entry point) and are not included in further tracking. Next a special Deflector Program tracks the surviving rays through the second electrostatic deflector (E2) and through the array of inert magnetic elements to the cyclotron exit port. (This program computes the median plane field of the magnetic elements point-by-point using the saturated steel approximation and computes off median plane fields to first order using the first derivatives of the median plane field.) Figure 4 shows an envelope plot from the Deflector Program for the 1390 rays which cleared the E1 septum, plotted vs. path-length from the point where they enter E1 through E2 and following magnetic focusing bars to the exit port of the

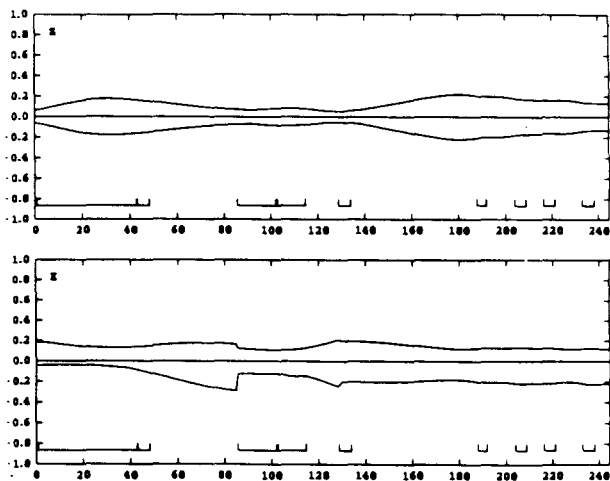


Figure 4: Axial and radial envelopes for the rays from figure 3 which enter the E1 deflector without hitting the septum and pass through the remaining extraction elements to the K1200 exit port. Upper trace is the symmetric axial envelope, lower is the radial envelope both in inches.

cyclotron. The step decreases in the x envelope correspond to losses at points where the available aperture changes (such as at the entrance to E2 at  $s = 84$ ", etc.). In this example a total of 145 rays (8.1%) are lost along the extraction trajectory so that 1245 rays or 69.7% of the initial 1785 ray ensemble finally successfully exit the cyclotron. This efficiency approximately matches the upper end of the range of values achieved in carefully tuned runs in the actual cyclotron.

## 2.4 Orbit Centering Effects

Figure 5 is like Figure 1 except that the centering coils have been deliberately set to produce a coherent radial oscillation. Looking first at the first full precession loop in the Figure we see that the amplitude of the induced centering error is considerably larger for the  $200^\circ$  starting time ray (the lowest ray in the Figure) than for the  $220^\circ$  ray at the top in the Figure. This is due to phase dependent effects in the central region. On the very first turns the energy gain at successive accelerating gaps varies greatly depending on the phase, and centering is thereby shifted but this effect is substantially the same for the centered rays shown in Figure 1 as for the off center rays shown in Figure 5. The main difference between the rays shown in the two Figures occurs at the central region  $v_r = 1$  crossing. At this resonance, the non-isochronism of the central focusing cone, has shifted the starting time group fully to one side of the rf wave. This then gives an energy gain per turn at the resonance which is smallest for the  $200^\circ$  ray, and successively larger for each succeeding ray in the group. As the group of rays reaches the second  $v_r = 1$  transition in the vicinity of 38.8", an additional radial amplitude component is introduced. This component adds

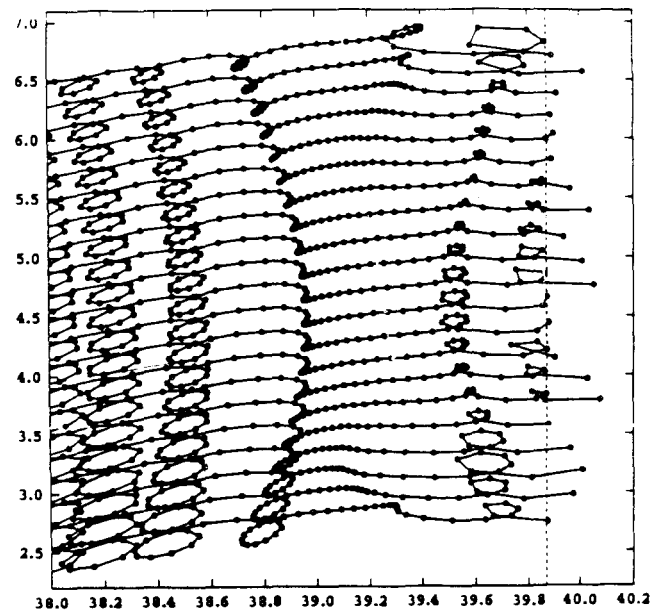


Figure 5: Plot of the same family of central rays as in Figure 1 except that the centering coil has been readjusted to produce a coherent centering error of approximately 0.075" amplitude (1.9 mm).

vectorially to the component induced at the central region resonance crossing, the differing phases of the two components leading to a rapidly varying highly disorganized final oscillation as seen in the 39.6" to 39.8" radius region, and for corresponding conditions septum losses are nearly doubled. Losses in the remainder of the extraction channel are also greatly increased as discussed in the following section.

### 3 Summary of Results

The principle results of this study are summarized in Table 1 which shows basic parameters, septum losses, and overall extraction efficiency for a set of ten large ensemble runs delineating various features of the multi-turn extraction process. A first surprising result is shown in the first three entries (ID labels A, B, & C). These sets of runs differ only by a small change in the dee voltage such that the 210° degree "central" central ray lines up on the middle of the deflector aperture on its last turn in A, just on the septum in its last turn in C and half way between these two values in the last turn of B. The purpose of this set of runs was to test the sensitivity of the multi-turn mode to the voltage stability of the rf system. The surprising result (unlike single turn extraction) is that septum losses for the three ensembles are virtually the same, and set C, where the 210° ray is lined up to hit the septum dead on, actually gives slightly lower losses. This is a totally opposite result from that which would result for single-turn extraction where A would give the highest efficiency, C the lowest and B in between. The surprising conclusion: extreme rf stability is not important in the multi-turn mode.

Another interesting comparison is between lines A and J which differ in that "large r" particles are included in A but not in J. Subtracting the J particles from A leaves a residual efficiency for "large r" of 57% i.e. a loss rate x2.3 higher for "large r" particles than for "small r".

The study described here, at this point in time, considers only the K1200 in "stand-alone" mode. Further work will assess performance of coupled mode operation in comparable detail. One can however draw some general conclusions regarding the 90% extraction goal of the coupled cyclotron project[6], namely, 1) effective septum thickness will need to be in the 0.1 mm range, 2) radial and axial emittances will both need to be in the 3 mm-mr range, and 3) the beam will need to be well centered. Item 1) is possibly accomplished by using a "notch" in a somewhat thicker septum (detailed consideration of a notch geometry is at present beyond the scope of our codes. Item 2) can clearly be accomplished with appropriate slits in the K500 injection line and in the coupling line, but higher ion source brightness will be required. Item 3) requires careful steering of the injected beam onto the accelerated equilibrium orbit corresponding to the K500 extraction energy. These are clearly non-trivial issues which will require careful work to achieve. The insensitivity of the broad-phase, multi-turn mode to space charge effects and to small rf voltage variations is, however, a compelling advantage favoring that operating mode.

**Acknowledgements.** This work is supported by the US National Science Foundation grant PHY-95-28844.

### References

- [1] Marti et al, proceedings of this conference
- [2] Poe et al, proceedings of this conference
- [3] Heidenreich & Stambach, Proc 9<sup>th</sup> Int'l Conf on Cyc & Their Applications p.369(1981)
- [4] Blosser et al, Proc 1997 Part Accel Conf, Vancouver (in press)
- [5] M. M. Gordon & V. Taivassalo, NIM A247(1986)423
- [6] York et al, proceedings of this conference

Table 1: Major parameters and results for 10 of the large ray ensembles ( denoted by the ID letters A,B, ..... J ). Radial and axial emittances are given as full areas without the frequently used factor of  $\pi$ , so that 12 mm-mr in the Table is the same as  $3.8 \pi$  mm-mr, etc. Entries in the last column – "Extraction Efficiency to Exit (%)" are all computed using a 0.5 mm septum thickness. For all runs the deflector aperture is 6.0 mm throughout its length and the deflector shape has been adjusted to approximately balance exit-end losses on the large radius side of the septum and the small radius side of the high voltage electrode.

ID	Dee Volts (kV)	Centered Beam?	Radial Emittance (mm-mr)	Axial Emittance (mm-mr)	First Deflector Septum Loss (%)			Extraction Efficiency to Exit (%)
					Septum thk. 0.125 mm	Septum thk. 0.25 mm	Septum thk. 0.50 mm	
A	106.15	Yes	3 + 12	3	11.8	15.9	22.1	69.7
B	106.19	Yes	3 + 12	3	11.0	14.8	22.1	
C	106.23	Yes	3 + 12	3	9.2	13.6	21.3	
D	106.15	Yes	3 + 12	12	17.0	21.0	28.3	58.2
E	106.15	No	3 + 12	3	23.3	28.0	37.0	
F	106.23	No	3 + 12	3	24.1	29.2	38.5	
G	106.15	No	3 + 12	12	39.3	43.0	49.9	
H	106.15	No	3	3	18.1	23.4	34.9	
I	106.15	No	3	12	37.6	41.9	50.5	32.3
J	106.15	Yes	3	3				81.1